ISSN 8755-6839

SCIENCE OF **TSUNAMI HAZARDS**

Journal of Tsunami Society International

Volume 41 Number 3 2022

GLACIAL LAKE TSUNAMI OF 13 OCTOBER 2000 ON "EL ALTAR" VOLCANO OF ECUADOR

Theofilos Toulkeridis[1]*, Izar Sínde-González[1] and Jheny Orbe[2]

[1]Universidad de las Fuerzas Armadas ESPE, Sangolquí, Ecuador
[2]Escuela Superior Politécnica del Chimborazo (ESPOCH), Riobamba, Ecuador
*Corresponding author: ttoulkeridis@espe.edu.ec

ABSTRACT

There are a number of unusual tsunamis, which occur within the continents rather than in the oceans, named inland tsunamis. One of these rare occasions occurred in the morning of the Friday the 13th October 2000 in a volcanic glacial lake of the horseshoe shaped extinct El Altar volcano in central Ecuador. A detailed mapping of available air photos and satellite images have been reviewed and evaluated in order to reconstruct the catastrophic event of 2000 and a previous one, evidencing that climate change and the associated subsequent reduction of the glacial caps have been responsible for the disassociation of a huge mass of rock(s), of which separation has resulted to an impact in the volcanic lake by an almost free fall of some 770 meters above lake level ground. This impact generated a tsunami wave capable to reach an altitude of 125 meters about the lake´s water level and leave to lower grounds killing some ten people and hundreds of animals with a mixture of a secondary lahar and debris avalanche. We tried to explain how the fall has occurred with some theoretical considerations, which resulted to imply that the rock hit at least once, probably twice the caldera wall prior lake impact. Such phenomena, even if rare, need to be better monitored in order to avoid settlements in potential areas in the reach of such devastating waves and subsequent avalanches, even more so, when due to climate change the accumulation of water in such lakes increases and the corresponding subglacial erosion and corresponding disassociation of lose rock material may set free more rocks with substantial volumes.

Keywords: *Inland tsunami, glacial lake, climate change, public preparedness, Ecuador*

1. INTRODUCTION

Tsunamis are usually known to be triggered by tectonic movements mostly along active continental margins (Pararas-Carayannis, 2006; 2012; Sulli et al., 2018; Zaniboni et al., 2014). The worldwide majority of tsunamis and their coastal impacts occur in the Pacific region, of which some prominent events caused enormous economic damage and or caused a relatively high death toll, like the tsunami of Sumatra in 2004, in Chile in 2010 and in Japan in 2011 (Fujii & Satake, 2007; Borrero & Greer, 2013; Nohara, 2011; Mori et al., 2011). A further way to generate tsunamis is attributed to volcanic activity which sometimes realize their subsequent marine or submarine mass movements due to flank or volcanic dome collapses, like those of occurred in Santorini in Late Bronze age, Unzen in 1792, Krakatau in 1883, Anak Krakatau in 2018, and of Hunga Tonga-Hunga Ha'apai in 2022 (Self & Rampino, 1981; Nomikou et al., 2016; Paris, 2015; Grilli et al., 2019; Sassa et al., 2016; Toulkeridis et al., 2022). Especially the dome collapse of Unzen volcano triggered a giant wave with a height of some 100 meters (Wang et al., 2019; Sassa et al., 2014).

Mass movements including iceberg collapses in oceanic environments have generated in the past often mega tsunamis also known as Iminamis with prominent examples such as Storegga in Norway, Big Island Hawaii, Teide in the Canaries, Roca Redonda in the Galapagos, Lituya Bay in Alaska, among many others (Bondevik et al., 1997; McMurtry et al., 2004; Paris et al., 2017; Cando et al., 2006; Kawamura et al., 2014; Völker et al., 2012; Greene & Ward, 2003; Harbitz et al., 2014; Mader & Gittings, 2002; Fritz et al., 2009; Ward & Day, 2010; Franco et al., 2020; Pararas-Carayannis, 1999; González-Vida et al., 2019). A fourth way to trigger tsunamis by natural processes occurred when space objects have impacted earth in an oceanic or sea environment like the famous impact in Yucatan, which accelerated mass extinction of most living species in the Cretaceous-Tertiary boundary, when the impact of an asteroid generated also a tsunami (Ward & Asphaug, 2000; Kharif & Pelinovsky, 2005; Hills & Mader, 1997; Matsui et al., 2002; Schulte et al., 2010; Kinsland et al., 2021; Kring, 2007; Glimsdal et al., 2007; Toulkeridis et al., 2021).

Nonetheless, besides the most known way to trigger tsunamis, by seismic activity, volcanic hazards, marine or submarine mass movements and impact of space objects in oceanic or sea environments, there is one more form of tsunami generation which occurs when a large amount of water displacement is caused by a sudden addition of material into a
body of water like lakes. Therefore, when such tsunamis occur due to a sudden landslide or rock fall, they are named inland tsunamis (Hilbe & Anselmetti, 2015; Kremer et al., 2021). Some prominent examples are those occurred in the Mount St Helens volcano in 1980, when a wave with a height of some 260 was generated by a lateral blast and corresponding debris avalanche, or, the one generated in Genoa, Italy in 1963, when rocks hit a water reservoir generating a tsunami height of some 25 meters (Ward & Day, 2006; Gawel et al., 2018; Semenza & Ghirotti, 2000; Genevois & Ghirotti, 2005; Paronuzzi & Bolla, 2012).

Due to an analysis of historic data and eye witness reports, we are able to add one more rare case of an inland tsunami, which occurred in Ecuador, within a volcanic glacier lake at an altitude of 4180 meters above sea level. This tsunami occurred on a Friday the 13th of October 2000 and the resulting wave killed some ten persons and hundreds of animals of the livestock. The current research will reconstruct the event and explain how it occurred and explain the probability of how a repetition may be generated in close future times.

2. GEOLOGIC AND GEOMORPHOLOGIC SETTING

Ecuador is situated along the easternmost margin of the Pacific ocean, where several tectonic plates are responsible for the actual geodynamic setting (Lebras et al., 1987; Daly, 1989; Jaillard et al., 2009; Toulkeridis et al., 2019; Luna et al., 2017). There is the conjunction of the Pacific, Cocos and Nazca oceanic plates as well as the Galapagos microplate besides their interaction with the Caribbean and South American continental plates (Fig.1) (Lonsdale, 1988; Klein et al., 2005; Pennington, 1981; Gailler et al., 2007). Out of this constellation result seismic movements with the generation of strong earthquakes and severe tsunamis as recorded in past history (Mendoza & Dewey, 1984; Sennson & Beck, 1996; Graindorge et al., 2004; Pararas-Carayannis & Zoll, 2017; Toulkeridis et al., 2017; Yamanaka et al., 2017; Pulido et al., 2020; Yoshimoto et al., 2017). There are several studies about Ecuador´s past tsunami impacts and associated seismic hazards, paleo-tsunami deposits, economic damages, prevention and mitigation efforts as well as the vulnerabilities of the public and the infrastructure (Chunga and Toulkeridis, 2014; Toulkeridis, 2016; Matheus Medina et al., 2016; Mato and Toulkeridis, 2017; Toulkeridis et al., 2017; Rodríguez Espinosa et al., 2017; Chunga et al., 2017; Toulkeridis et al., 2018; Mato and Toulkeridis, 2018; Navas et al., 2018; Celorio-Saltos et al., 2018; Matheus-Medina et al., 2018; Chunga et al., 2019; Toulkeridis et al., 2019; Martinez and Toulkeridis, 2020; Edler et al., 2020; Suárez-Acosta et al., 2021; Del-Pino-de-la-Cruz et al., 2021; Toulkeridis et al., 2021; Ortiz-Hernández et al., 2022; Aviles-Campoverde et al., 2021). These studies also handled the impacts and corresponding responses of public and authorities have been studied of tsunamis regional and far-triggered origins such as those of Chile in 2010, Japan in 2011 and Tonga in 2022 on the continental shores of Ecuador as well as on their Galapagos Islands.

A high amount of volcanoes appear in Ecuador and the Galapagos Islands as a result of the subduction of the Nazca plate below the continent which gives rise on a variety of volcanoes aligned on NNE-SSW direction of four almost parallel lines forming different volcanic chains and the Galapagos hot spot, the latter responsible for the formation of the more than 3000 volcanoes in the Galapagos (Toulkeridis & Angermeyer, 2019). In the continental part, there are more than 250 volcanoes distributed in the Western Volcanic Cordillera (WC),

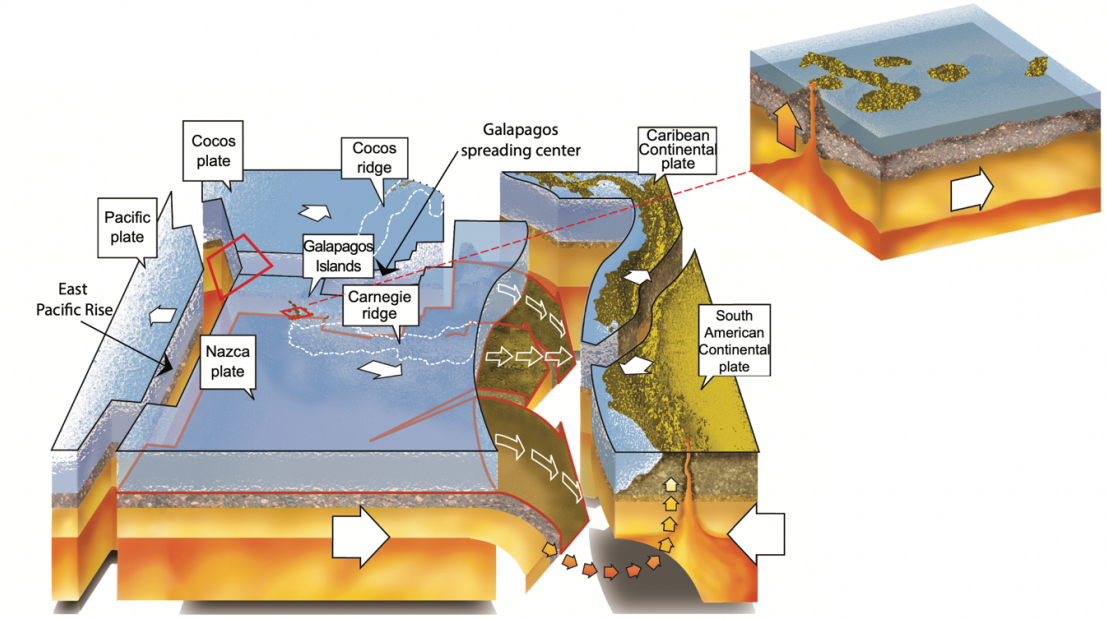

Fig. 1. The geodynamic situation of Ecuador and associated plates, micro-plates and volcanic ridges. The Guayaquil-Caracas Mega Fault is situated within the separation of the Caribbean and South American Continental Plates. The Galapagos microplate occurs in the triple junction between the three oceanic plates (red square).

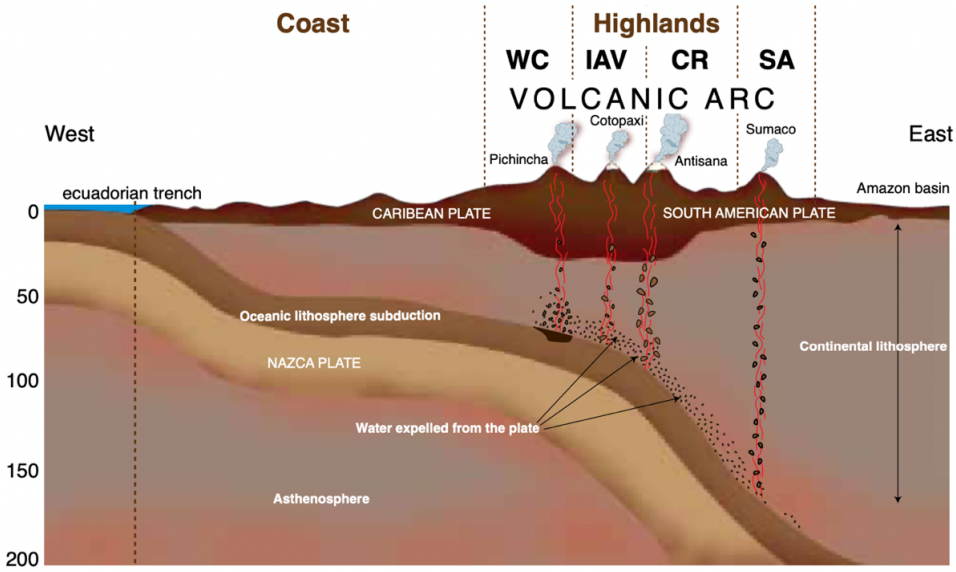

Fig. 2: Schematic profile from west to east within the subduction zone and the respective volcanic areas. WC = Western cordillera; IAV = Interandean valley; CR = Cordillera Real; SA = SubAndean region.

the Inter-Andean Volcanic Cordillera (IAV), the Eastern Volcanic Cordillera (CR), which is situated above the Cordillera Real and the easternmost Sub-Andean Volcanic Cordillera (SA) (Fig. 2). Of all these volcanoes, some 19 are considered to be active and occasionally very dangerous including a super volcano named Chalupas (Toulkeridis et al., 2007; Ridolfi et al., 2008; Padrón et al., 2008; 2012; Toulkeridis et al., 2015; Rodriguez et al., 2017; Toulkeridis and Zach, 2017; Melián et al., 2021).

The El Altar volcano, also known locally as Cápac Urcu (the mighty one or the lord of the volcanoes), being part of the Eastern Volcanic Cordillera is considered an extinct volcano since the middle Pleistocene. The maximum height of this volcano named El Obispo (The Bishop) reaches some 5,319 m.a.s.l., being one of seven prominent peaks, which are named El Canónico, Los Frailes, El Tabernáculo, La Monja Menor, La Monja Mayor, El Acólito (The Canon, The Friars, The Tabernacle, The Minor Nun, The Major Nun, The Acolyte). The horseshoe-shaped volcano is open to its west, as a result of a giant collapse (Fig. 3, 4). In its inner part, the caldera is composed of a gabbroic intrusion, which most likely represents a part of the magma chamber, besides andesitic and rhyolitic lavas and dikes, of which many are brecciated, especially in the upper part of the edifice.

3. THE CATASTROPHIC EVENT AND ITS POTENTIAL THEORETICAL RECONSTRUCTION

According to local witnesses, shortly before 6 a.m., in the morning of Friday the 13th of October 2000, a giant explosive sound was heard from the inner part of the volcano. Shortly after, a giant water wave overflow the fifty meters high wall from the western side of the glacial Lake Laguna Amarilla forming downstream a debris avalanche in the Valley of Collanes within the Río Blanco river, until it reached the confluence with the Río Tarau river. According to Civil Defense reports at the time, more than 400 families were affected, 10 people disappeared, 10 homes were destroyed, while 200 head of cattle were lost and some 600 hectares of crops were destroyed.

Based on topographic maps realized prior and after the year 2000, together with satellite images, and additional studies and observations in the field, it was determined that a piece of the inner wall of the volcano collapsed in the form of a rock from a height of 4955 meters above sea level (m.a.s.l.). This has been the initial tear-off edge and the whole lose part reached up to 5070 m.a.s.l., being its higher end some 230 meters below the peak in that part of the volcano. This loosening has occurred in the northern part of the peak called Monja Grande. The size of this rock wall was of about 115 meters high, about 90 meters wide and 35 meters thick in its widest part, so the maximum dimensions of the lost rock wall were then 115x90x35 meters. The rock, being an andesite breccia in this formation of the volcano, has had a density of 2.5–2.8 t/m^3, which means of having had a maximum weight of some 905,625 tons. This weight, although massive is just a tiny part compared with similar events, where in 1958, some 30,6 million cubic meter of rocks impacted the ocean in Lituya Bay Alaska, generating a tsunami wave height of some 524 meters (Mader & Gittings, 2002).

This piece of rock crashed at least once at a height of approximately 4640 meters above sea level, before hitting the lagoon. It is very likely that with this drop of about 315 meters, the rock broke, potentially splitting into two or more pieces of unknown proportions. From the initial tear edge to this crash it had a horizontal distance of maximum 260 meters. From that impact height of about 4640 meters, the rock(s) either fell into the lagoon or crashed again at a lower height but before the level of the lagoon before impacting in it. From this crash point to the edge of the lagoon we determined a horizontal distance of about 440 meters. The surface of the lake is approximately 4,182 meters above sea level. The maximum observable height of the subsequent tsunami wave has been of about 125 meters above the lagoon level, that is, more or less 4,310 meters above sea level, eroding the local moraine deposits.

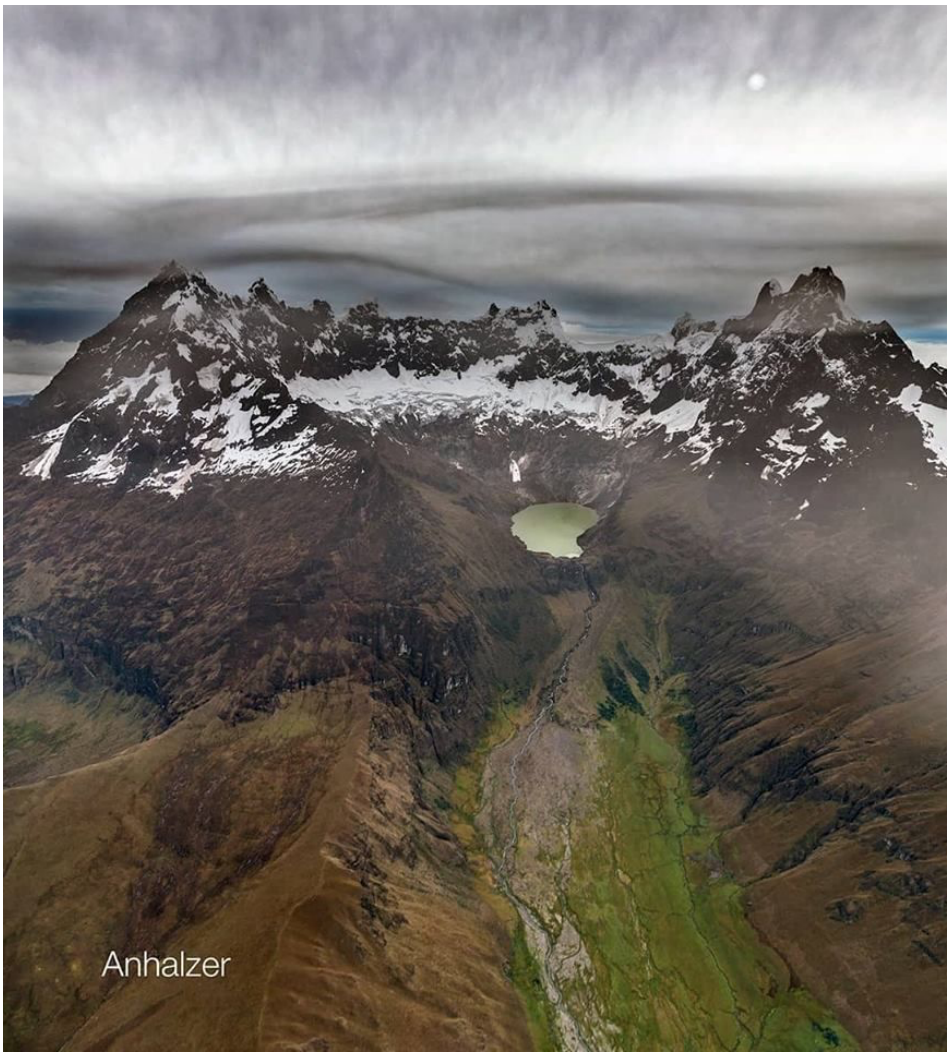

Figure 3. The horseshoe-shaped El Altar volcano, open towards west, with its glacial lake, the Laguna Amarilla. The Moja Grande peak is the second peak from right to left. Photo credit by Jorge Anhalzer.

When the giant wave overflow of the inland tsunami reached the Río Blanco river, the water got mixed and pushed the loose rocks of previous glacial deposits and other volcanic materials forming a debris avalanche. This avalanche reached the Río Tarau river, where a first damming of the waters occurred. Besides the deaths and the previously described destruction, an 800-meter section of the highway that connects Penipe with La Candelaria also disappeared, as well as the bridge that crosses the Blanco River where another damming of water, mud and rocks took place. Later, the muddy avalanche crossed the rivers Chambo and Pastaza reaching later the Amazonian basin on sites like Puyo and beyond. The rise of the debris material was also noted in the Hydroagoyan water plant further downstream, where even the timing of the arrival has been reported.

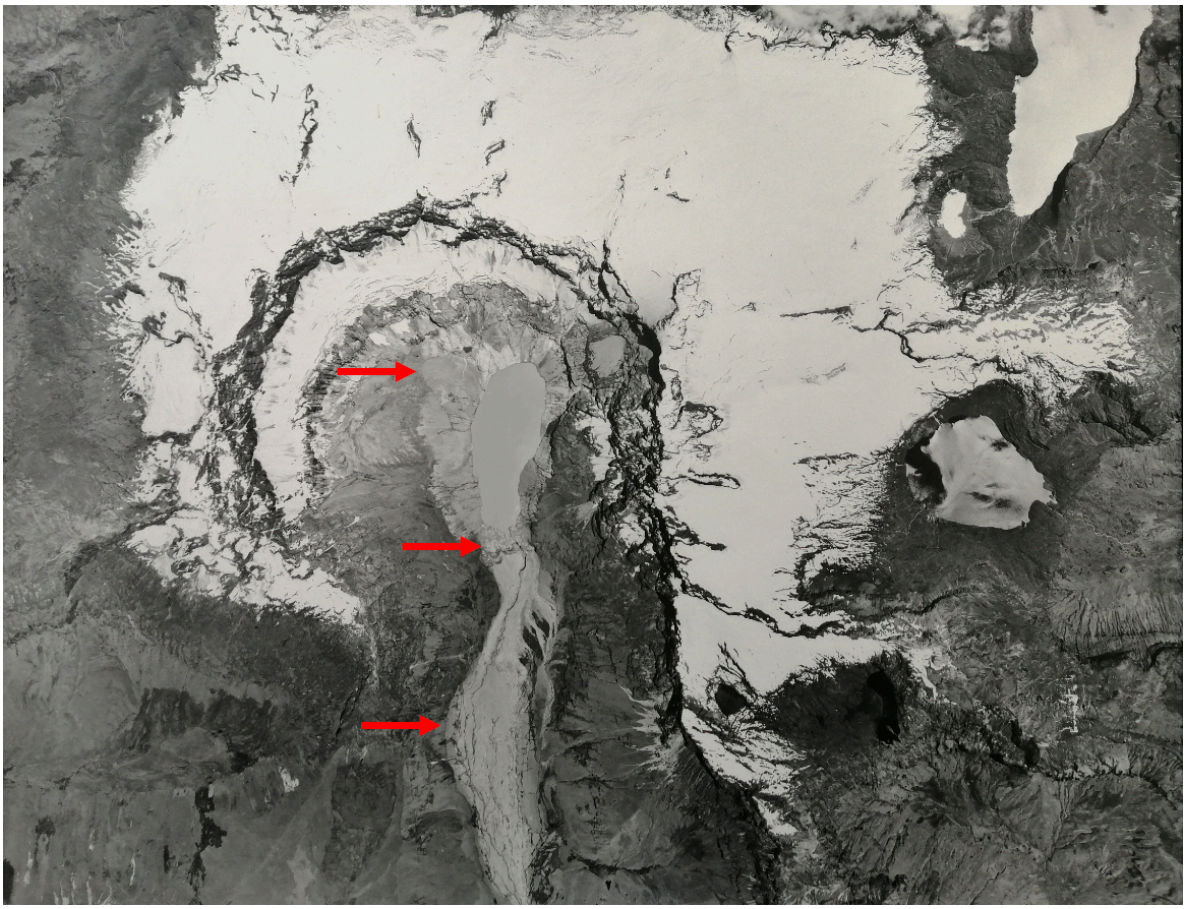

Figure 4. Two weeks after the event was taken this orthophoto from the Ecuadorian Military Geographical Institute (IGM), where we are able to evidence and proof the field observations, demonstrating the highest run-up at a 4,310 m.a.s.l. (upper arrow) at the northern inner caldera wall, the western lake barrier, being 50 meters higher than the lake water level (middle arrow) and the extension of the debris avalanche in the Valley of Collanes (lower arrow). North is on the left, while south is on the right of the black and white picture. Photo credit by IGM.

In order to reconstruct the fall and impact of the rock and its resulting giant tsunami wave within the lagoon, we used simple mathematical and physical considerations. In this sense we applied the known parameters, which are the rock size, its density and corresponding weight on the one hand, and on the other the known height of the wave. Hereby, the rock in free fall from a height of 773 meters is assumed, taking the surface of the lagoon as a reference system, if the initial velocity is zero, it will impact with an edge of the volcano's profile, located 315 meters below the point of detachment, with a maximum horizontal distance of 260 from the initial edge. All the aforementioned parameters were determined with a relative error of 2%. Therefore, the arrival time at the collision point is of about 8.0 ± 0.2 seconds (Equation 1), with a speed of approximately 78.6 ± 0.8 m/s (Equation 2).

$$t = \sqrt{\frac{2h}{g}} \qquad (1)$$

$$v_0 = \sqrt{2gh} \qquad (2)$$

Where:

t = elapsed time for the rock to reach the edge of the collision

h= height from the point of detachment of the rock to the point of collision with the edge

g = acceleration due to gravity

v_0 = speed of arrival of the rock at the collision point

Several trajectories of descent of the rock to the lagoon can be assumed, but in order to quantify some specific physical parameters of the phenomenon (time, speed, range, acceleration), two cases in which the rock is divided into two identical fragments, the collision is assumed elastic and the subsequent motion of the fragments is studied in two dimensions.

A) First Case

Figure 5 illustrates the situation prior and after the collision of the rock with the edge, while the velocities of the fragments generate equal angles with the horizontal.

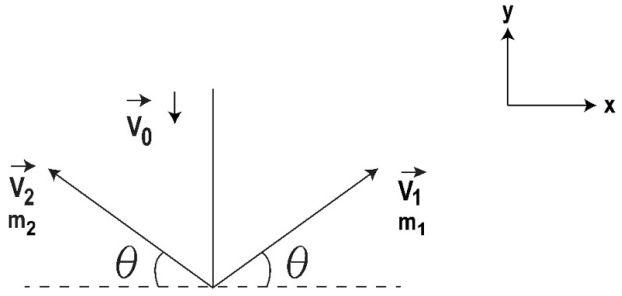

Figure 5: Collision of the rock with the edge, dividing it into two equal fragments with positive velocities on the y-axis.

The law of conservation of momentum is applied before and after the collision (Equation 3). The initial speed of the fragments is the same (Equation 4) and was calculated using Equation 5.

$$\vec{p}_0 = \vec{p}_f \qquad (3)$$

$$m_1 = m_2 = \frac{m}{2}$$

$$m\vec{v}_0 = \frac{m}{2}\vec{v}_1 + \frac{m}{2}\vec{v}_2$$

$$2\vec{v}_0 = \vec{v}_1 + \vec{v}_2$$

X direction:

$$0 = v_1 cos\theta - v_2 cos\theta$$

$$v_1 = v_2 \qquad (4)$$

Y direction:

$$-2v_{0y} = v_1 sen\theta + v_2 sen\theta$$

$$-2v_{0y} = 2v_1 sen\theta$$

$$v_1 = -\frac{v_{0y}}{sen\theta} = -\frac{v_0}{sen\theta} \qquad (5)$$

Where:
$\vec{p}_0$ = amount of movement before the collision
$\vec{p}_f$ = momentum after collision
m = rock mass
m_1 = mass of fragment 1
m_2 = mass of fragment 2
$\vec{v}_1$ = speed of fragment 1
$\vec{v}_2$ = speed of fragment 2
$\vec{v}_0$ = velocity vector of arrival of the rock at the collision point
θ = angle that the velocities of the fragments make with the horizontal

Figure 6 illustrates the case of fragment 1, thrown into the air with an angle θ and an initial speed $\vec{v}_1$, when it moves freely under the action of gravity only (air resistance is not considered). The acceleration of the rock fragment, acting downward, is 9.8 m/s^2. Motion is assumed to start when time equals zero (t=0) at the origin of a coordinate system, so $x_0=y_0=0$.

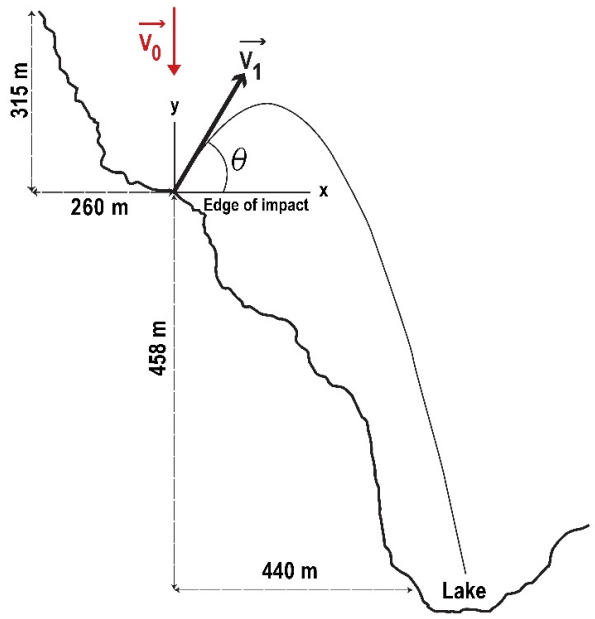

Figure 6. Trajectory of fragment 1 fired with an initial velocity $\vec{v}_1$ forming an angle θ (positive) with the edge plane.

The rock rise time to the maximum height was calculated with Equation (6). The maximum height that the rock reaches in the air was evaluated with Equation (7).

$$t_s = \frac{v_{0y}}{g} \qquad (6)$$

$$v_{0y} = v_0$$

$$h_{max} = h_i + v_0 t_s \qquad (7)$$

Where:

t_s = rock rise time

v_{0y} = component of the velocity of the rock on the y-axis

h_{max} = maximum height that the rock reaches in the air

h_i = height from the shock point to the plane of the lagoon

The rock fall time from the maximum height to the lagoon surface is a parameter that was quantified with Equation (8). The time of flight is the total time of the rock in the air and was calculated with Equation (9).

$$t_c = \sqrt{\frac{2h_{max}}{g}} \qquad (8)$$

$$t_v = t_s + t_c \qquad (9)$$

Where:

$t_c =$ rock fall time from the maximum height to the lagoon plane

$t_v =$ time of flight

The horizontal distance that the rock travels from the point of impact to the point of arrival at the lagoon or at the ground (reach) was evaluated with Equation (10). The horizontal distance from the edge of the lagoon to the impact point of the rock was calculated with Equation (11).

$$x = v_{1x}\, t_v \qquad (10)$$

$$v_{1x} = \frac{v_1}{\text{sen}\theta}\cos\theta$$

$$v_{1x} = v_1 \cot\theta$$

$$x_i = x - x_b \qquad (11)$$

Where:

x_i = distance from the edge of the lagoon to the point of impact of the rock in the water

$x_b =$ horizontal distance from the point of rock collision to the edge of the lagoon

v_{1x} = component of the initial velocity on the x axis

x = reach.

The final speed with which the rock impacts the surface of the lagoon was calculated with Equation (12):

$$v_{1f} = \sqrt{v_{1xf}^2 + v_{1yf}^2} \qquad (12)$$

$$v_{1xf} = v_{1x}$$

$$v_{1yf} = g\, t_v$$

Where:
v_{1f} = final velocity of the rock upon reaching the water
$v_{1yf=}$ final velocity in y-direction
v_{1xf} = final velocity in the x direction

Considering that the lagoon is 1,186 m long and 575 m wide, dimensions estimated with a relative uncertainty of 2%, it is observed that for launch angles in the range of 62 - 76 degrees. Hereby, the rock experiences a flying time of 22.9 ± 0.1 seconds, when it reaches a maximum height of 1088 ± 10 m and hits the surface of the lagoon at 57 ± 3 m from the right edge and 9.0 ± 0.5 m from the left edge, respectively, taking as reference system the one indicated in Figure 6. Therefore, the impact speed is of about 248 ± 2 m/s. For a launch angle of 68 degrees, the rock lands half the width of the pond. For angles less than 62 and greater than 76 degrees, the rock does not impact the lagoon.

B) Second Case

Figure 7 illustrates the situation prior and after the collision of the rock with the edge of the volcano profile. The velocities of the fragments form equal negative angles with the horizontal. Hereby, equations 3 and 4 are applicable to this case, while the initial velocity of the fragments was calculated using Equation 13.

Y direction:

$$-2v_{0y} = -v_1 sen\theta - v_2 sen\theta$$

$$2v_{0y} = 2v_1 sen\theta$$

$$v_1 = \frac{v_{0y}}{sen\theta} = \frac{v_0}{sen\theta} \quad (13)$$

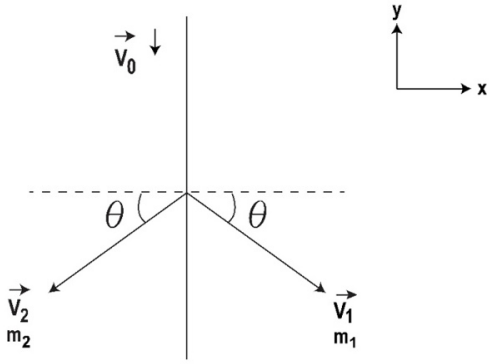

Figure 7: Collision of the rock with the edge, dividing it into two equal fragments with negative velocities on the y-axis.

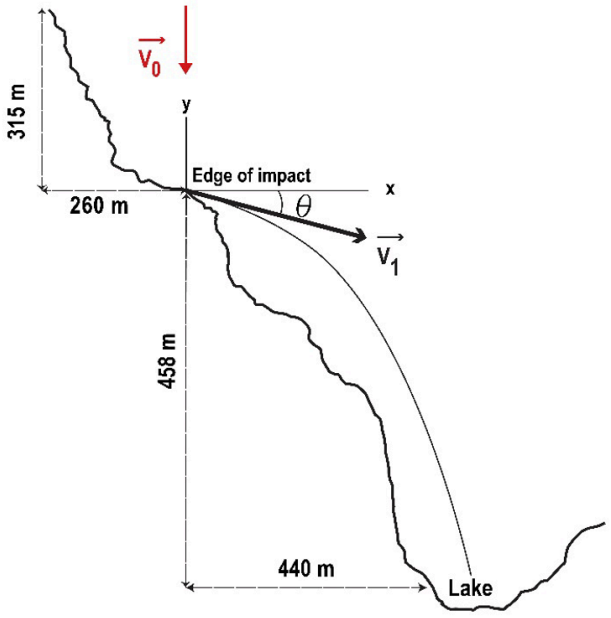

Figure 8. Trajectory of fragment 1 fired with an initial velocity $\vec{v}_1$ forming an angle θ (negative) with the edge plane.

Figure 8 presents the case of fragment 1, launched into the air with an angle θ (negative) and an initial speed $\vec{v}_1$. There is no rise time for the rock, while the initial velocity on the vertical axis is negative (in the same direction as gravity). The maximum height is the vertical distance between the point of impact and the surface of the lagoon (458 m). Equations 10 and 11 were used to calculate the reach and arrival point of the rock to the ground or the lagoon, respectively.

The final speed with which the rock hits the surface of the lagoon was calculated with Equation (14)

$$v_{1f} = \sqrt{v_{1xf}^2 + v_{1yf}^2} \quad (14)$$

$$v_{1xf} = v_{1x}$$

$$v_{1yf} = g\,t_v + v_{1y}$$

Where:

v_{1y} = component of the initial velocity on the y-axis

For launch angles in the range 37 - 59 degrees, the rock experiences a flying time of 9.7 ± 0.5 seconds, impacting the lagoon surface with 7 ± 0.4 m from the right edge and 9 ± 0.5 m from the left edge, respectively, considering the one indicated in Figure 8 as the reference system. Therefore, the impact speed is of about 202 ± 2 m/s. For a launch angle of 47 degrees, the rock falls about half the width of the lagoon. For angles less than 37 and greater than 59 degrees, the rock does not impact the lagoon.

In both cases presented, fragment 2 that starts with speed $\vec{v}_2$ will collide with the slope of the volcano until it reaches the lagoon.

The dimensions of the entire rock were estimated with an uncertainty of 2%, considering a height of 115 meters high, width of about 90 meters and a thickness of about 35 meters, so the volume was calculated as a cube, resulting in a value of 362250 ± 21735 m^3. According to Archimedes' principle, when the rock impacts, the surface of the lagoon will displace a volume of water equal to the volume of the rock, if a cylindrical column is considered, the water will reach a height given by equations 15 and 16.

$$V = \pi r^2 h \qquad (15)$$

$$h = \frac{V}{\pi r^2} \qquad (16)$$

Where:

r = radius of the water column

V = volume of displaced water

h = height of the water column

In this context, it is evident that the height of the water wave in the lagoon (as a function of the radius of the column) is independent of the trajectory during the descent and only depends on whether it arrived whole or in fragments. If the rock arrived as a whole, it would form a 125 ± 8 m column with a radius of 30.3 m. Taking this radius as a reference, if the rock was divided into two, three and four parts, each fragment would form a water column with a height of 62.7 ± 4 m, 41.8 ± 3 m and 31.3 ± 2 m, respectively.

4. CLIMATE CHANGE AS POTENTIAL TRIGGER?

Such catastrophic event based on al inland tsunami seems not to be the first occurring in this site. In 1953 impacted a similar event the less filled lake of El Altar, generating also an overflow and subsequently a debris avalanche in the Valley of Collanes. However, the impact has been of much less proportions as the lake has been in its beginning process of upfilling due to the initial stage of glacial reduction. In fact, explorers reported in the 18th century, that the glaciers occupied the entire interior of the caldera and also reached the upper slopes of the Valle de Collanes. That leads to the preliminary hypothesis, that lose rocks have been generated due to physical weathering in such subglacial environment, where due to glacial reduction based on the contemporaneous climate change such lose and or brecciated rock fragments followed gravity leading to a catastrophe such as those of Friday the 13th nightmare of the inland tsunami disaster at El Altar volcano in October 2000 (Toulkeridis et al., 2020).

Glacial retreat or reduction is a worldwide phenomenon which is interpreted as a direct result of global warming and climate change (Kaser et al., 2004; Byg & Salick, 2009; Roe EtAl, 2017; Bolch, 2007). The resulting landscape has often tremendous consequences for the aquatic system, the flora

and fauna, the society as well as industry (Magnuson et al., 1997; Allison, 2017; Omambia & Gu, 2010). The reduction of glacial icecaps are contributing to a slow but steady worldwide sea level rise and sometimes often to sudden hazardous lake developments (Vilímek et al., 2005; Richardson & Reynolds, 2000; Emmer et al., 2014; Stuart-Smith et al., 2021).

In Ecuador, the accelerated reduction of glacial ice-covers on volcanoes and mountains is visible since the last century, while some of them disappeared completely. The remaining glaciers are limited to the peaks of Antisana, Cotopaxi, Chimborazo, Cayambe, Los Ilinizas (north and south), Carihuairazo and El Altar. In order to demonstrate and evidence the shrinkage of the El Altar volcano glacier, various images were downloaded from the Landsat satellites (Landsat 5, Landsat 7 and Landsat 8). In table 1, a summary is listed about the most fundamental characteristics of each image.

Table 1. Satellites Images of the studied area

Image date	Satellite	Cloud cover	Spatial resolution
1991/07/27	Landsat 5	29.00%	30 m.
1998/07/14	Landsat 5	9.00%	
2007/07/31	Landsat 7*	29.00 %	
2016/11/20	Landsat 8	19.81 %	

* In the case of the Landsat 7 image, a banding correction was applied

As a next step, in order to quantify the reduction in the size of the glacier over the years, the digitization of the glacier was conducted, with the support of a composition (SWIR, RED, GREEN), which corresponds to bands 5-3-2 for Landsat 5 and 7 satellites and bands 6-4-3 for Landsat 8 satellite. Hereby, we compared the shape of the glacier over several years with the corresponding compositions as illustrated in figure 9. Subsequently, to quantify the retreat of the glacier at different times, a polygon was digitized for each image, through which the surface of each of them could be calculated. This digitization and the surface of each glacier can be evidenced in figure 10.

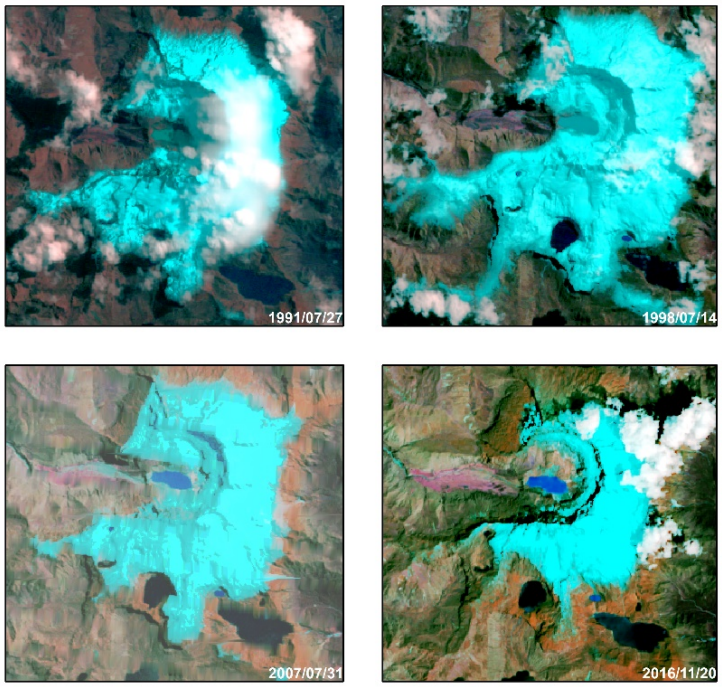

Figure 9. Composition (SWIR, RED, GREEN), of four different times in the Altar volcano.

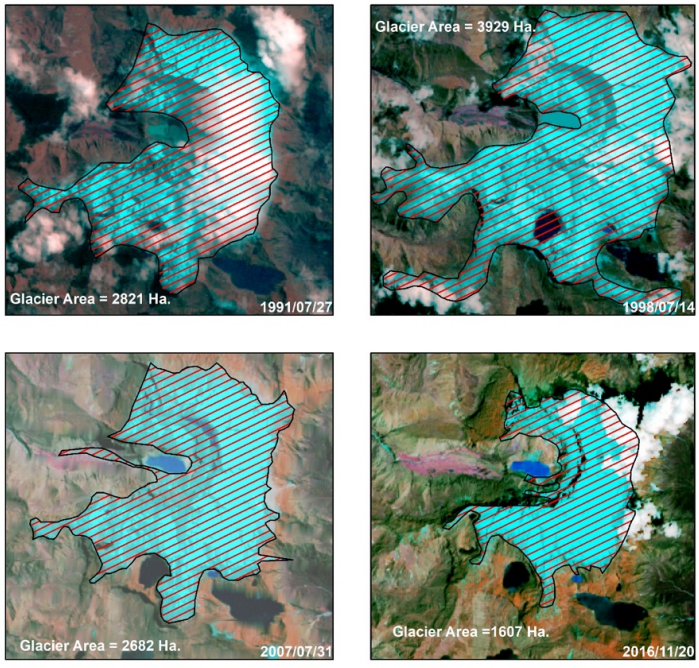

Figure 10. Quantification of El Altar´s glacial reduction between 1991 and 2016.

5. CONCLUSIONS

A combination of various circumstances has been responsible for the rare inland tsunami of the Friday the 13th of October 2000 in the extinct volcano El Altar, situated in the Eastern Volcanic Cordillera of the Ecuadorian Andes. These conditions included physical weathering in a subglacial environment, reduction of the glacial icecaps and the subsequent accumulation of meltwater in the lower parts of the volcano within an up-filling lake.

All these aforementioned circumstances are related to the evident climate change and thus will have even stronger repetitions in the near future due to an increase of extreme conditions as seen in other parts of the world.

Generally, the public preparedness in Ecuador does not coincide with the occurring natural events as catastrophic as they may have been, which leads to the conclusion, that a better awareness and education needs to be developed by the corresponding authorities.

6. REFERENCES

Allison, E. A. (2015). The spiritual significance of glaciers in an age of climate change. Wiley Interdisciplinary Reviews: Climate Change, 6(5), 493-508.

Aviles-Campoverde, D., Chunga, K., Ortiz-Hernández, E., Vivas-Espinoza, E., Toulkeridis, T., Morales-Delgado, A. and Delgado-Toala, D. (2021). Seismically induced soil liquefaction and geological conditions in the city of Jama due to the Mw7.8 Pedernales earthquake in 2016, NW Ecuador. Geosciences, 11, 20

Bolch, T. (2007). Climate change and glacier retreat in northern Tien Shan (Kazakhstan/Kyrgyzstan) using remote sensing data. Global and Planetary Change, 56(1-2), 1-12.

Bondevik, S., Svendsen, J. I., Johnsen, G., Mangerud, J. A. N., & Kaland, P. E. (1997). The Storegga tsunami along the Norwegian coast, its age and run up. Boreas, 26(1), 29-53.

Borrero, J. C., & Greer, S. D. (2013). Comparison of the 2010 Chile and 2011 Japan tsunamis in the far field. Pure and Applied Geophysics, 170(6), 1249-1274.

Byg, A., & Salick, J. (2009). Local perspectives on a global phenomenon—climate change in Eastern Tibetan villages. Global environmental change, 19(2), 156-166.

Cando, M., Arreaga, P., Toulkeridis, T., & De La Torre, G. (2006). Evidences for potential future sector collapse at Volcano Roca Redonda, northern Galápagos—Tectonics, simulation and consequences, paper presented at 4th Meeting, Cities on Volcanoes. Int. Assoc. of Volcanol. and Chem. of the Earth's Inter., Quito, Ecuador, 23-27.

Celorio-Saltos, J.C., García-Arias, J.M., Guerra-Luque, A.B., Barragan-Aroca, G. and Toulkeridis, T. (2018). Vulnerability analysis based on tsunami hazards in Crucita, central coastal of Ecuador. Science of Tsunami Hazards, 38(3): 225-263.

Chunga, K. and Toulkeridis, T. (2014). First evidence of paleo-tsunami deposits of a major historic event in Ecuador. Science of tsunami hazards, 33: 55-69.

Chunga, K., Mulas, M., Alvarez, A., Galarza, J. and Toulkeridis, T. (2019). Characterization of seismogenetic crustal faults in the Gulf of Guayaquil, Ecuador. Andean Geology, 46(1): 66-81.

Chunga, K., Toulkeridis, T., Vera-Grunauer, X., Gutierrez, M., Cahuana, N. And Alvarez, A. (2017). A review of earthquakes and tsunami records and characterization of capable faults on the northwestern coast of Ecuador. Science of tsunami hazards, 36: 100-127.

Daly, M. C. (1989). Correlations between Nazca/Farallon plate kinematics and forearc basin evolution in Ecuador. Tectonics, 8(4), 769-790.

Del-Pino-de-la-Cruz, C.E., Martinez-Molina, B.D., Haro-Baez, A.G., Toulkeridis, T. and Rentería, W. (2021). The proposed design of a smart parking area as a multiple use building for the eventual vertical evacuation in case of tsunami impacts in Salinas, Ecuador. Science of Tsunami Hazards, 40(3), 146-165.

Edler, D., Otto, K.H and Toulkeridis, T. (2020). Tsunami hazards in Ecuador – Regional differences in the knowledge of Ecuadorian high-school students. Science of Tsunami Hazards, 39(2), 86-112.

Emmer, A., Vilímek, V., Klimeš, J., & Cochachin, A. (2014). Glacier retreat, lakes development and associated natural hazards in Cordilera Blanca, Peru. In Landslides in cold regions in the context of climate change (pp. 231-252). Springer, Cham.

Franco, A., Moernaut, J., Schneider-Muntau, B., Strasser, M., & Gems, B. (2020). The 1958 Lituya Bay tsunami–pre-event bathymetry reconstruction and 3D numerical modelling utilising the computational fluid dynamics software Flow-3D. Natural Hazards and Earth System Sciences, 20(8), 2255-2279.

Fritz, H. M., Mohammed, F., & Yoo, J. (2009). Lituya Bay landslide impact generated mega-tsunami 50 th Anniversary. In Tsunami Science Four Years after the 2004 Indian Ocean Tsunami (pp. 153-175). Birkhäuser Basel.

Fujii, Y., & Satake, K. (2007). Tsunami source of the 2004 Sumatra–Andaman earthquake inferred from tide gauge and satellite data. Bulletin of the Seismological Society of America, 97(1A), S192-S207.

Gailler, A., Charvis, P., & Flueh, E. R. (2007). Segmentation of the Nazca and South American plates along the Ecuador subduction zone from wide angle seismic profiles. Earth and Planetary Science Letters, 260(3-4), 444-464.

Gawel, J. E., Crisafulli, C. M., & Miller, R. (2018). The New Spirit Lake: Changes to Hydrology, Nutrient Cycling, and Biological Productivity. In Ecological Responses at Mount St. Helens: Revisited 35 years after the 1980 Eruption (pp. 71-95). Springer, New York, NY.

Genevois, R., & Ghirotti, M. (2005). The 1963 vaiont landslide. Giornale di Geologia Applicata, 1(1), 41-52.

Glimsdal, S., Pedersen, G. K., Langtangen, H. P., Shuvalov, V., & Dypvik, H. (2007). Tsunami generation and propagation from the Mjølnir asteroid impact. Meteoritics & Planetary Science, 42(9), 1473-1493.

González-Vida, J. M., Macías, J., Castro, M. J., Sánchez-Linares, C., de la Asunción, M., Ortega-Acosta, S., & Arcas, D. (2019). The Lituya Bay landslide-generated mega-tsunami–numerical simulation and sensitivity analysis. Natural Hazards and Earth System Sciences, 19(2), 369-388.

Graindorge, D., Calahorrano, A., Charvis, P., Collot, J. Y., & Bethoux, N. (2004). Deep structures of the Ecuador convergent margin and the Carnegie Ridge, possible consequence on great earthquakes recurrence interval. Geophysical Research Letters, 31(4).

Greene, H. G., & Ward, S. N. (2003). Mass movement features along the central California margin and their modeled consequences for tsunami generation. In Submarine Mass Movements and Their Consequences (pp. 343-356). Springer, Dordrecht.

Grilli, S. T., Tappin, D. R., Carey, S., Watt, S. F., Ward, S. N., Grilli, A. R., ... & Muin, M. (2019). Modelling of the tsunami from the December 22, 2018 lateral collapse of Anak Krakatau volcano in the Sunda Straits, Indonesia. Scientific reports, 9(1), 1-13.

Harbitz, C. B., Løvholt, F., & Bungum, H. (2014). Submarine landslide tsunamis: how extreme and how likely?. Natural Hazards, 72(3), 1341-1374.

Hilbe, M., & Anselmetti, F. S. (2015). Mass movement-induced tsunami hazard on perialpine Lake Lucerne (Switzerland): scenarios and numerical experiments. Pure and Applied Geophysics, 172(2), 545-568.

Hills, J. G., & Mader, C. L. (1997). Tsunami produced by the impacts of small asteroids. Annals of the New York Academy of Sciences, 822(1), 381-394.

Jaillard, E., Lapierre, H., Ordonez, M., Alava, J. T., Amortegui, A., & Vanmelle, J. (2009). Accreted oceanic terranes in Ecuador: southern edge of the Caribbean Plate?. Geological Society, London, Special Publications, 328(1), 469-485.

Kaser, G., Hardy, D. R., Mölg, T., Bradley, R. S., & Hyera, T. M. (2004). Modern glacier retreat on Kilimanjaro as evidence of climate change: observations and facts. International Journal of Climatology: A Journal of the Royal Meteorological Society, 24(3), 329-339.

Kawamura, K., Laberg, J. S., & Kanamatsu, T. (2014). Potential tsunamigenic submarine landslides in active margins. Marine Geology, 356, 44-49.

Kharif, C., & Pelinovsky, E. (2005). Asteroid impact tsunamis. Comptes Rendus Physique, 6(3), 361-366.

Kinsland, G. L., Egedahl, K., Strong, M. A., & Ivy, R. (2021). Chicxulub impact tsunami megaripples in the subsurface of Louisiana: Imaged in petroleum industry seismic data. Earth and Planetary Science Letters, 570, 117063.

Klein, E. M., Smith, D. K., Williams, C. M., & Schouten, H. (2005). Counter-rotating microplates at the Galapagos triple junction. Nature, 433(7028), 855-858.

Kremer, K., Anselmetti, F. S., Evers, F. M., Goff, J., & Nigg, V. (2021). Freshwater (paleo) tsunamis–a review. Earth-science reviews, 212, 103447.

Kring, D. A. (2007). The Chicxulub impact event and its environmental consequences at the Cretaceous–Tertiary boundary. Palaeogeography, Palaeoclimatology, Palaeoecology, 255(1-2), 4-21.

Lebras, M., Megard, F., Dupuy, C., & Dostal, J. (1987). Geochemistry and tectonic setting of pre-collision Cretaceous and Paleogene volcanic rocks of Ecuador. Geological Society of America Bulletin, 99(4), 569-578.

Lonsdale, P. (1988). Structural pattern of the Galapagos microplate and evolution of the Galapagos triple junctions. Journal of Geophysical Research: Solid Earth, 93(B11), 13551-13574.

Luna, M. P., Staller, A., Toulkeridis, T., & Parra, H. (2017). Methodological approach for the estimation of a new velocity model for continental Ecuador. Open Geosciences, 9(1), 719-734.

Mader, C. L., & Gittings, M. L. (2002). Modeling the 1958 Lituya Bay mega-tsunami, II. Science of Tsunami Hazards, 20(5), 241-250.

Magnuson, J. J., Webster, K. E., Assel, R. A., Bowser, C. J., Dillon, P. J., Eaton, J. G., ... & Quinn, F. H. (1997). Potential effects of climate changes on aquatic systems: Laurentian Great Lakes and Precambrian Shield Region. Hydrological processes, 11(8), 825-871.

Martinez, N. and Toulkeridis, T. (2020). Tsunamis in Panama – History, preparation and future consequences. Science of Tsunami Hazards, 39(2), 53-68.

Matheus Medina, A.S., Cruz D´Howitt, M., Padilla Almeida, O., Toulkeridis, T. and Haro, A.G. (2016). Enhanced vertical evacuation applications with geomatic tools for tsunamis in Salinas, Ecuador. Science of Tsunami Hazards, 35, (3): 189-213

Matheus-Medina, A.S., Toulkeridis, T., Padilla-Almeida, O., Cruz-D´Howitt, M. and Chunga, K. (2018). Evaluation of the tsunami vulnerability in the coastal Ecuadorian tourist centers of the peninsulas of Bahia de Caráquez and Salinas. Science of Tsunami Hazards, 38(3): 175-209.

Mato, F. and Toulkeridis, T. (2017). The missing Link in El Niño's phenomenon generation. Science of tsunami hazards, 36: 128-144.

Mato, F. and Toulkeridis, T. (2018). An unsupervised K-means based clustering method for geophysical post-earthquake diagnosis. 2017 IEEE Symposium Series on Computational Intelligence (SSCI). 1-8

Matsui, T., Imamura, F., Tajika, E., Nakano, Y., & Fujisawa, Y. (2002). Generation and propagation of a tsunami from the Cretaceous-Tertiary impact event. SPECIAL PAPERS-GEOLOGICAL SOCIETY OF AMERICA, 69-78.

McMurtry, G. M., Watts, P., Fryer, G. J., Smith, J. R., & Imamura, F. (2004). Giant landslides, mega-tsunamis, and paleo-sea level in the Hawaiian Islands. Marine Geology, 203(3-4), 219-233.

Melián, G.V., Toulkeridis, T., Pérez, N.M., Hernández Pérez, P.A., Somoza, L., Padrón, E., Amonte, C., Alonso, M., Asensio-Ramos, M. and Cordero, M. (2021). Geochemistry of water and gas emissions from Cuicocha and Quilotoa Volcanic Lakes, Ecuador. Frontiers in Earth Sciences, 1167

Mendoza, C., & Dewey, J. W. (1984). Seismicity associated with the great Colombia-Ecuador earthquakes of 1942, 1958, and 1979: Implications for barrier models of earthquake rupture. Bulletin of the seismological society of America, 74(2), 577-593.

Mori, N., Takahashi, T., Yasuda, T., & Yanagisawa, H. (2011). Survey of 2011 Tohoku earthquake tsunami inundation and run−up. Geophysical research letters, 38(7).

Navas, L., Caiza, P. and Toulkeridis, T. (2018). An evaluated comparison between the molecule and steel framing construction systems – Implications for the seismic vulnerable Ecuador. Malaysian Construct. Res. J. 26 (3), 87–109.

Nohara, M. (2011). Impact of the Great East Japan Earthquake and tsunami on health, medical care and public health systems in Iwate Prefecture, Japan, 2011. Western Pacific Surveillance and Response Journal: WPSAR, 2(4), 24.

Nomikou, P., Druitt, T. H., Hübscher, C., Mather, T. A., Paulatto, M., Kalnins, L. M., ... & Parks, M. M. (2016). Post-eruptive flooding of Santorini caldera and implications for tsunami generation. Nature communications, 7(1), 1-10.

Omambia, C. S., & Gu, Y. (2010). The cost of climate change in Tanzania: impacts and adaptations. Journal of American Science, 6(3), 182-196.

Ortiz-Hernández, E., Chunga, K. Pastor, J.L. and Toulkeridis, T. (2022). Assessing susceptibility to soil liquefaction, using the standard penetration test (SPT) – A case study from the city of Portoviejo, coastal Ecuador. Land, online

Ortiz-Hernández, E., Chunga, K. Toulkeridis, T. and Pastor, J.L. (2022). Soil liquefaction and other seismic-associated phenomena in the city of Chone during the 2016 earthquake of coastal Ecuador. Applied Science, online

Padrón, E., Hernández, P.A., Marrero, R., Melián, G, Toulkeridis, T., Pérez., N.M., Virgili, G. and Notsu, K. (2008). Diffuse CO2 emission rate from the lake-filled Cuicocha and Pululagua calderas, Ecuador. Journal of Volcanology and Geothermal Research (Special Volume on Continental Ecuador volcanoes), 176: 163-169.

Padrón, E., Hernández, P.A., Pérez, N.M., Toulkeridis, T., Melián, G., Barrancos, J., Virgili, G., Sumino H. and Notsu, K. (2012). Fumarole/plume and diffuse CO2 emission from Sierra Negra volcano, Galapagos archipelago. Bull. Of Volcanol., 74: 1509-1519.

Pararas-Carayannis, G. (1999). Analysis of mechanism of tsunami generation in Lituya Bay. Science of Tsunami Hazards, 17(3), 193-206.

Pararas-Carayannis, G. (2006). The potential of tsunami generation along the Makran Subduction Zone in the northern Arabian Sea: Case study: The earthquake and tsunami of November 28, 1945. Science of Tsunami Hazards, 24(5), 358-384.

Pararas-Carayannis, G. (2012). Potential of tsunami generation along the Colombia/Ecuador subduction margin and the Dolores-Guayaquil mega-thrust. Science of Tsunami Hazards, 31(3), 209-230

Pararas-Carayannis, G., & Zoll, P. (2017). Incipient evaluation of temporal El Nino and other climatic anomalies in triggering earthquakes and tsunamis-Case Study: The Earthquake and Tsunami of 16 th April 2016 in Ecuador. Science of Tsunami Hazards, 36(4), 262-291

Paris, R. (2015). Source mechanisms of volcanic tsunamis. Phil. Trans. R. Soc. A 373, 20140380.

Paris, R., Bravo, J. J. C., González, M. E. M., Kelfoun, K., & Nauret, F. (2017). Explosive eruption, flank collapse and megatsunami at Tenerife ca. 170 ka. Nature Communications, 8(1), 1-8.

Paronuzzi, P., & Bolla, A. (2012). The prehistoric Vajont rockslide: an updated geological model. Geomorphology, 169, 165-191.

Pennington, W. D. (1981). Subduction of the eastern Panama Basin and seismotectonics of northwestern South America. Journal of Geophysical Research: Solid Earth, 86(B11), 10753-10770.

Pulido, N., Yoshimoto, M., & Sarabia, A. M. (2020). Broadband wavelength slip model of the 1906 Ecuador-Colombia megathrust-earthquake based on seismic intensity and tsunami data. Tectonophysics, 774, 228226.

Richardson, S. D., & Reynolds, J. M. (2000). An overview of glacial hazards in the Himalayas. Quaternary International, 65, 31-47.

Ridolfi, F., Puerini, M., Renzulli, A., Menna, M. and Toulkeridis, T. (2008). The magmatic feeding system of El Reventador volcano (Sub-Andean zone, Ecuador) constrained by mineralogy, textures and geothermobarometry of the 2002 erupted products. Journal of Volcanology and Geothermal Research (Special Volume on Continental Ecuador volcanoes), 176: 94-106.

Rodríguez Espinosa, F., Toulkeridis, T., Salazar Martinez, R., Cueva Girón, J., Taipe Quispe, A., Bernaza Quiñonez, L., Padilla Almeida, O., Mato, F., Cruz D´Howitt, M., Parra, H., Sandoval, W. and Rentería, W. (2017). Economic evaluation of recovering a natural protection with concurrent relocation of the threatened public of tsunami hazards in central coastal Ecuador. Science of tsunami hazards, 36: 293-306.

Rodriguez, F., Toulkeridis, T., Padilla, O. and Mato, F. (2017). Economic risk assessment of Cotopaxi volcano Ecuador in case of a future lahar emplacement. Natural Hazards, 85, (1): 605-618.

Roe, G. H., Baker, M. B., & Herla, F. (2017). Centennial glacier retreat as categorical evidence of regional climate change. Nature Geoscience, 10(2), 95-99.

Sassa, K., Dang, K., He, B., Takara, K., Inoue, K., & Nagai, O. (2014). A new high-stress undrained ring-shear apparatus and its application to the 1792 Unzen–Mayuyama megaslide in Japan. Landslides, 11(5), 827-842.

Sassa, K., Dang, K., Yanagisawa, H., & He, B. (2016). A new landslide-induced tsunami simulation model and its application to the 1792 Unzen-Mayuyama landslide-and-tsunami disaster. Landslides, 13(6), 1405-1419.

Schulte, P., Alegret, L., Arenillas, I., Arz, J. A., Barton, P. J., Bown, P. R., ... & Willumsen, P. S. (2010). The Chicxulub asteroid impact and mass extinction at the Cretaceous-Paleogene boundary. Science, 327(5970), 1214-1218.

Self, S. & Rampino, M. R. (1981). The 1883 eruption of Krakatau. Nature 294, 699–704.

Semenza, E., & Ghirotti, M. (2000). History of the 1963 Vaiont slide: the importance of geological factors. Bulletin of Engineering Geology and the Environment, 59(2), 87-97.

Sennson, J. L., & Beck, S. L. (1996). Historical 1942 Ecuador and 1942 Peru subduction earthquakes and earthquake cycles along Colombia-Ecuador and Peru subduction segments. Pure and applied geophysics, 146(1), 67-101.

Stuart-Smith, R. F., Roe, G. H., Li, S., & Allen, M. R. (2021). Increased outburst flood hazard from Lake Palcacocha due to human-induced glacier retreat. Nature Geoscience, 14(2), 85-90.

Suárez-Acosta, P.E., Cañamar-Tipan, C.D., Ñato-Criollo, D.A., Vera-Zambrano, J.D., Galarza-Vega, K.L., Guevara-Álvarez, P.M., Fajardo-Cartuche, C.N., Herrera-Garcés, K. K., Ochoa-Campoverde, C.V., Torres-Orellana, J.S., Rentería, W., Chunga, K., Padilla, O., Sinde-González, I., Simón-Baile, D. and Toulkeridis, T. (2021). Evaluation of seismic and tsunami resistance of potential shelters for vertical evacuation in case of a tsunami impact in Bahia de Caráquez, central coast of Ecuador. Science of Tsunami Hazards, 40(1), 1-37.

Sulli, A., Zizzo, E., & Albano, L. (2018). Comparing methods for computation of run-up heights of landslide-generated tsunami in the Northern Sicily continental margin. Geo-Marine Letters, 38(5), 439-455.

Toulkeridis, T. (2013). Volcanes Activos Ecuador. Santa Rita, Quito, Ecuador: 152 pp

Toulkeridis, T. (2016). The Evaluation of unexpected results of a seismic hazard applied to a modern hydroelectric center in central Ecuador. Journal of Structural Engineering, 43, (4): 373-380.

Toulkeridis, T. and Angermeyer, H. (2019). Volcanoes of the Galapagos. 2nd Edition, Abad Offest, Guayaquil, Ecuador: 324pp

Toulkeridis, T. and Zach, I. (2017). Wind directions of volcanic ash-charged clouds in Ecuador – Implications for the public and flight safety. Geomatics, Natural Hazards and Risks, 8(2): 242-256.

Toulkeridis, T., Arroyo, C.R., Cruz D'Howitt, M., Debut, A., Vaca, A.V., Cumbal, L., Mato, F. and Aguilera, E. (2015). Evaluation of the initial stage of the reactivated Cotopaxi volcano - Analysis of the first ejected fine-grained material. Natural Hazards and Earth System Sciences, 3, (11): 6947-6976.

Toulkeridis, T., Barahona-Quelal, I.N., Pilco-Paguay, E.O., Cacuango-Casco, D.M., Guilcaso-Tipán, B.S. and Sailema-Hurtado, W.P. (2021). Evaluation of seismic and tsunami resistance of potential shelters for vertical evacuation in case of a tsunami impact in Manta and Salinas, central coast of Ecuador. Science of Tsunami Hazards, 40(4), 286-314.

Toulkeridis, T., Buchwaldt, R. and Addison, A. (2007). When Volcanoes Threaten, Scientists Warn. Geotimes, 52: 36-39.

Toulkeridis, T., Chunga, K., Rentería, W., Rodriguez, F., Mato, F., Nikolaou, S., Cruz D´Howitt, M., Besenzon, D., Ruiz, H., Parra, H. and Vera-Grunauer, X. (2017). The 7.8 Mw Earthquake and Tsunami of the 16th April 2016 in Ecuador - Seismic evaluation, geological field survey and economic implications. Science of tsunami hazards, 36: 197-242.

Toulkeridis, T., Echegaray-Aveiga, R.C. and Martinez-Maldonado, K.P. (2021) Shock metamorphism in volcanic rock due to the impact of the Miguir-Cajas meteorite in 1995 and its importance for Ecuador. Geojournal of Tourism and Geosites, 35(2), 315-321.

Toulkeridis, T., Martinez, N., Barrantes, G., Rentería, W., Barragan-Aroca, G., Simón-Baile, D., Palacios, I., Salazar, R., Salcedo-Hurtado, E.d.J. and Pararas-Carayannis, G. (2022). Impact and response in Central and South America due to the tsunami generated by the submarine eruption of Hunga Tonga-Hunga Ha'apai volcano. Science of Tsunami Hazards, 41(1), 1-38.

Toulkeridis, T., Mato, F., Toulkeridis-Estrella, K., Perez Salinas, J.C., Tapia, S. and Fuertes, W. (2018). Real-Time Radioactive Precursor of the April 16, 2016 Mw 7.8 Earthquake and Tsunami in Ecuador. Science of tsunami hazards, 37: 34-48.

Toulkeridis, T., Parra, H., Mato, F., Cruz D´Howitt, M., Sandoval, W., Padilla Almeida, O., Rentería, W., Rodríguez Espinosa, F., Salazar Martinez, R., Cueva Girón, J., Taipe Quispe, A. and Bernaza Quiñonez, L. (2017). Contrasting results of potential tsunami hazards in Muisne, central coast of Ecuador. Science of tsunami hazards, 36: 13-40

Toulkeridis, T., Porras, L., Tierra, A., Toulkeridis-Estrella, K., Cisneros, D., Luna, M., ... & Salazar, R. (2019). Two independent real-time precursors of the 7.8 Mw earthquake in Ecuador based on radioactive and geodetic processes—Powerful tools for an early warning system. Journal of Geodynamics, 126, 12-22.

Toulkeridis, T., Porras, L., Tierra, A., Toulkeridis-Estrella, K., Cisneros, D., Luna, M., Carrión, J.L., Herrera, M., Murillo, A., Perez-Salinas, J.C., Tapia, S., Fuertes, W. and Salazar, R. (2019). A potential early warning system for earthquakes based on two independent real-time precursors – the case of Ecuador´s 7.8 Mw in 2016. Proceedings of the International Conference on Natural Hazards and Infrastructure 2019, 2nd International Conference on Natural Hazards and Infrastructure, ICONHIC 2019; Chania; Greece; 23 June 2019 through 26 June 2019; Code 257429

Toulkeridis, T., Tamayo, E., Simón-Baile, D., Merizalde-Mora, M.J., Reyes –Yunga, D.F., Viera-Torres, M. and Heredia, M. (2020) Climate change according to Ecuadorian academics– Perceptions versus facts. La Granja, 31(1), 21-49

Vilímek, V., Zapata, M. L., Klimeš, J., Patzelt, Z., & Santillán, N. (2005). Influence of glacial retreat on natural hazards of the Palcacocha Lake area, Peru. Landslides, 2(2), 107-115.

Völker, D., Geersen, J., Behrmann, J. H., & Weinrebe, W. R. (2012). Submarine mass wasting off Southern Central Chile: distribution and possible mechanisms of slope failure at an active continental margin. In Submarine mass movements and their consequences (pp. 379-389). Springer, Dordrecht.

Wang, J., Ward, S. N., & Xiao, L. (2019). Tsunami Squares modeling of landslide generated impulsive waves and its application to the 1792 Unzen-Mayuyama mega-slide in Japan. Engineering Geology, 256, 121-137.

Ward, S. N., & Asphaug, E. (2000). Asteroid impact tsunami: a probabilistic hazard assessment. Icarus, 145(1), 64-78.

Ward, S. N., & Day, S. (2006). Particulate kinematic simulations of debris avalanches: interpretation of deposits and landslide seismic signals of Mount Saint Helens, 1980 May 18. Geophysical Journal International, 167(2), 991-1004.

Ward, S. N., & Day, S. (2010). The 1958 Lituya bay landslide and tsunami—A tsunami ball approach. Journal of Earthquake and Tsunami, 4(04), 285-319.

Yamanaka, Y., Tanioka, Y., & Shiina, T. (2017). A long source area of the 1906 Colombia–Ecuador earthquake estimated from observed tsunami waveforms. Earth, Planets and Space, 69(1), 1-11.

Yoshimoto, M., Kumagai, H., Acero, W., Ponce, G., Vásconez, F., Arrais, S., ... & Nakano, M. (2017). Depth‐dependent rupture mode along the Ecuador‐Colombia subduction zone. Geophysical Research Letters, 44(5), 2203-2210.

Zaniboni, F., Armigliato, A., Pagnoni, G., & Tinti, S. (2014). Continental margins as a source of tsunami hazard: The 1977 Gioia Tauro (Italy) landslide–tsunami investigated through numerical modeling. Marine Geology, 357, 210-217.